Mechanical mixing in nonlinear nanomechanical resonators

A. Erbe, H. Krömmer, A. Kraus, and R. H. Blick[a)]
Center for NanoScience and Sektion Physik, Ludwig-Maximilians-Universität, Geschwister-Scholl-Platz 1, 80539 München, Germany

G. Corso and K. Richter
Max-Planck-Institut für Physik komplexer Systeme, Nöthnitzer Strasse 38, 01187 Dresden, Germany

(Received 30 May 2000; accepted for publication 12 September 2000)

The physics of nonlinear dynamics has been studied in detail in macroscopic mechanical systems like the driven classical pendulum. By now, it is possible to build mechanical devices on the nanometer scale with eigenfrequencies on the order of several 100 MHz. In this work, we want to present how to machine such nanomechanical resonators out of silicon-on-insulator wafers and how to operate them in the nonlinear regime in order to investigate higher-order mechanical mixing at radio frequencies. The nonlinear response then is compared in detail to *n*th-order perturbation theory and nonperturbative numerical calculations. © *2000 American Institute of Physics.* [S0003-6951(00)04545-9]

Mechanical devices in combination with modern semiconductor electronics offer great advantages as, for example, their robustness against electrical shocks and ionization due to radiation. In the outstanding work by Rugar and Grütter,[1] the importance for applications in scanning-probe microscopy of mechanical cantilevers was demonstrated. Greywall *et al.*[2] investigated noise-evasion techniques for frequency sources and clocks. The main disadvantage of mechanical devices so far is the low speed of operation. This has been overcome with the realization of nanomechanical resonators, which allow operation at frequencies up to 500 MHz.[3–7]

In the present work, we realize such a nanomechanical resonator to study its nonlinear dynamics and its mechanical mixing properties. Mixing is of great importance for signal processing in common electronic circuits. Here, we present measurements on such a nonlinear nanomechanical resonator, forced into resonance by application of two different, but neighboring, driving frequencies. We also present a theoretical model, based on the Duffing equation, which accurately describes the behavior of the mechanical resonator.

The starting materials are commercially available silicon-on-insulator substrates with thicknesses of the Si layer and the SiO_2 sacrificial layer of 205 and 400 nm, respectively (Smart-Cut wafers). The gate leads connecting the resonator to the chip carrier are defined using optical lithography. In a next step, the nanomechanical resonator is defined by electron-beam lithography. The sample is dry etched in a reactive-ion etcher in order to obtain a mesa structure with clear-cut walls. Finally, we perform a hydrofluoric (HF) wet-etch step in order to remove the sacrificial layer below the resonators and the metallic etch mask. The suspended resonator is shown in a scanning electron-beam micrograph in Fig. 1(a): The beam has a length of $l=3\ \mu$m, a width of $w=200$ nm, and a height of $h=250$ nm, and is clamped on both sides. The inset shows a close up of the suspended beam. The restoring force of this Au/Si-hybrid beam is dominated by the stiffer Si supporting membrane.

The chip is mounted in a sample holder and a small amount of ^{4}He exchange gas is added (10 mbar) to ensure thermal coupling. The sample is placed at 4.2 K in a magnetic field, directed in parallel to the sample surface but perpendicular to the beam. When an alternating current is applied to the Au layer of the beam, a Lorentz force arises perpendicular to the sample surface and sets the beam into mechanical motion. For characterization, we employ a spec-

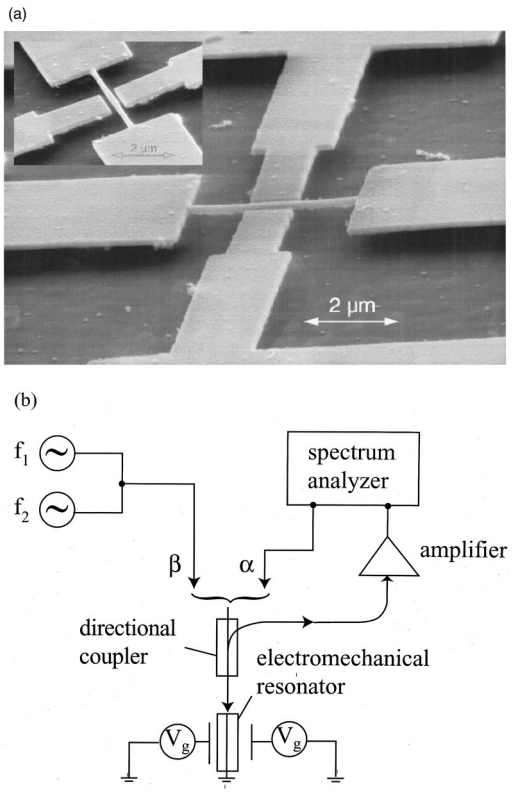

FIG. 1. (a) Scanning electron-beam micrograph of the electromechanical resonator with a length $l=3\ \mu$m, width $w=200$ nm, and height $h=250$ nm. The Si-supporting structure is covered by a thin Au sheet (50 nm thick); the electrodes on the left and right allow tuning of the elastic properties. Inset shows a view of the beam from a different angle. (b) Experimental setup for sampling the mechanical properties of the suspended beam: For characterization we employ a spectrum analyzer scanning the frequency range of interest (α). Mechanical mixing is analyzed by combining two synthesizers (f_1, f_2) and detecting the reflected power (β).

a)Electronic mail: robert.blick@physik.uni-muenchen.de

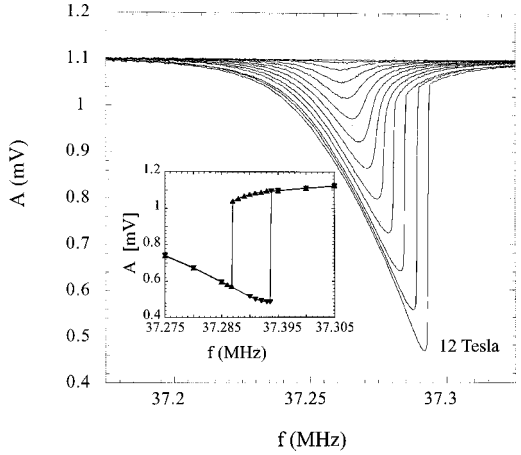

FIG. 2. Characterization of the nonlinear response of the suspended beam by ramping the magnetic field from 0 T up to 12 T, obtained with the spectrum analyzer operated with an output power level of −50 dBm (setup α). Inset shows the measured hysteresis: ▽ corresponds to an increase in frequency and △ represents the lowering branch.

trum analyzer (Hewlett Packard 8594A): The output frequency is scanning the frequency range of interest, the reflected signal is tracked, and then amplified [setup α in Fig. 1(b)]. The mixing properties of the suspended nanoresonators are probed with a different setup comprising two synthesizers (Marconi 2032 and Wavetek 3010) emitting excitations at constant, but different, frequency [setup β in Fig. 1(b)].

In Fig. 2 the radio-frequency response of the beam near resonance is depicted for increasing magnetic-field strength $B=0,1,2,...,12$ T. The excitation power of the spectrum analyzer was fixed at −50 dBm. The mechanical quality factor, $Q=f/\delta f$, of the particular resonator under test in the linear regime is $Q=2330$. As seen, the profile of the resonance curve changes from a symmetric shape at moderate fields to an asymmetric, sawtooth shape at large field values, characteristic of an oscillator operated in the nonlinear regime.

This behavior can be described by the Duffing equation

$$\ddot{x}(t)+\mu\dot{x}(t)+\omega_0^2 x(t)+\alpha x^3(t)=F(t), \tag{1}$$

with a positive prefactor α of the cubic term being the parameter of the strength of the nonlinearity.[8] In Eq. (1) μ is the damping coefficient of the mechanical system; $\omega_0=2\pi f_0$, where f_0 is the mechanical eigenfrequency of the beam; and $x(t)$ its displacement. In our case, the external driving $F(t)$ is given by the Lorentz force $F(t)=(lB/m_{\text{eff}})I_0\cos(2\pi ft)$, where $l=1.9\times10^{-6}$ m is the effective length and $m_{\text{eff}}=4.3\times10^{-16}$ kg is the effective mass of the resonator. B is the magnetic field and I_0 the input current.

Solving Eq. (1) and computing the amplitude of the oscillation as a function of the driving frequency f for several excitation strengths reproduces the measured curves shown in Fig. 2. The solutions at large power exhibit a region where three different amplitude values coexist at a single frequency. This behavior leads to a hysteretic response in the measurements at high powers (e.g., −50 dBm),[7] as shown in the inset of Fig. 2, where we used an external source (Marconi) to sweep the frequencies in both directions. If the frequency is increased [inverted triangles (▽) in the inset], the resonance first follows the lower branch, and then suddenly jumps to the upper branch. When sweeping downwards from higher to lower frequencies [triangles (△)], the jump in resonance occurs at a different frequency.

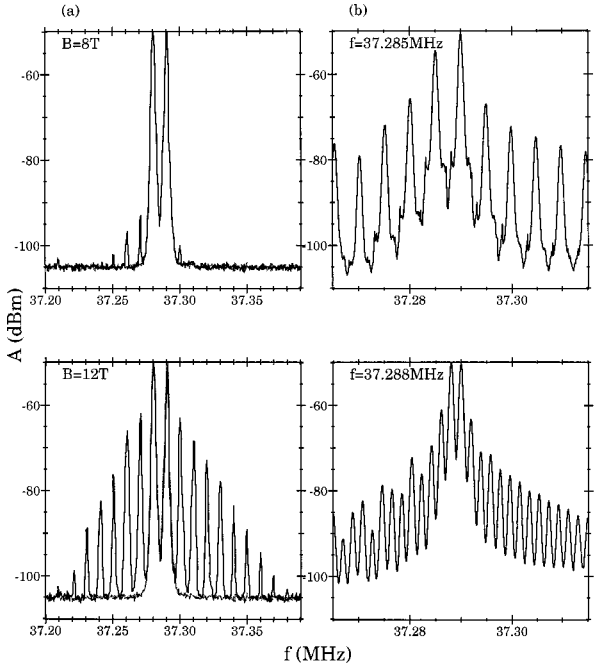

FIG. 3. (a) Two synthesizers [setup β in Fig. 1(b)] running at frequencies of $f_1=37.28$ MHz and $f_1=37.29$ MHz with constant offset (output power −48 dBm) induce higher-order harmonics as a result of mechanical mixing by the nanoresonator in the nonlinear regime ($B>8$ T). The gray line is taken at $B=0$ T, showing pure reflectance of the beam without excitation of mechanical motion. (b) Excitation with two frequencies at −48 dBm and $B=12$ T: Base frequency is $f_1=37.290$ MHz, while the sampling frequency $f_2=37.285$ and 37.288 MHz. As seen, the spacing of the harmonics follows the offset frequency $\Delta f=f_1-f_2$.

By applying two separate frequency sources, as sketched in Fig. 1(b) (setup β), it is possible to demonstrate mechanical mixing, as shown in Fig. 3(a). The two sources are tuned to $f_1=37.28$ MHz and $f_2=37.29$ MHz with constant offset and equal output power of −48 dBm, well in the nonlinear regime. Without applying a magnetic field, the two input signals are simply reflected. Crossing a critical field of $B\simeq8$ T, higher-order harmonics appear. Increasing the field strength further, a multitude of satellite peaks evolves. As seen, the limited bandwidth of this mechanical mixer allows effective signal filtering. The gray line is taken at zero field for comparison, showing only the reflected power when the beam is not set into mechanical motion.

Variation of the offset frequencies leads to the data presented in Fig. 3(b): Excitation at −48 dBm and $B=12$ T with the base frequency fixed at $f_1=37.290$ MHz and varying the sampling frequency in 1 kHz steps from $f_2=37.285$ to 37.290 MHz yields satellites at the offset frequencies $f_{1,2}\pm n\Delta f$, $\Delta f=f_1-f_2$. At the smallest offset frequency of 1 kHz the beam reflects the input signal as a broadband of excitations (data not shown).

We model the nanomechanical system as a Duffing oscillator (1) with a driving force

$$F(t)=F_1\cos(2\pi f_1 t)+F_2\cos(2\pi f_2 t), \tag{2}$$

with two different, but neighboring, frequencies f_1 and f_2 and amplitudes $F_i=lBI_i/m_{\text{eff}}$.

Before presenting our results of a numerical solution of Eq. (1) for the driving forces (2), we perform an analysis

based on nth-order perturbation theory[9] to explain the generation of higher harmonics. Expanding

$$x = x_0 + \epsilon x_1 + \epsilon^2 x_2 + \cdots, \tag{3}$$

where we assume that the (small) parameter ϵ is of order of the nonlinearity αx^3, and inserting this expansion into Eq. (1), yields equations for the different orders in ϵ. In zeroth order we have

$$\ddot{x}_0 + \mu \dot{x}_0 + \omega_0^2 x_0 = F_1 \cos(2\pi f_1 t) + F_2 \cos(2\pi f_2 t), \tag{4}$$

to first-order $\ddot{x}_1 + \mu \dot{x}_1 + \omega_0^2 x_1 + \alpha x_0^3 = 0$, and similar equations for higher orders. After inserting the solution of Eq. (4) into the first-order equation and assuming $f_1 \approx f_2 \approx f_0 = \omega_0/2\pi$, two types of peaks can be extracted: One peak is located at $3f_0$ which we, however, could not detect experimentally. Peaks of the other type are found at frequencies $f_i \pm \Delta f$. Proceeding along the same lines in second-order perturbation theory we obtain peaks at $5f_0$ and $f_i \pm 2\Delta f$. Accordingly, owing to the cubic nonlinear term, nth-order peaks are generated at $(2n+1)f_0$ and $f_i \pm n\Delta f$. While the $(2n+1)f_0$ peaks could not be observed, the whole satellite family $f_i \pm n\Delta f$ is detected in the experimental power spectra Figs. 3(a) and 3(b).

The perturbative approach yields the correct peak positions and, for $B < 4$ T, also the peak amplitudes. However, in the hysteretic, strongly nonlinear regime, a nonperturbative numerical calculation proves necessary to explain quantitatively the measured peak heights. To this end, we determined the parameters entering into Eq. (1) in the following way: The damping is estimated from the quality factor $Q = 2330$ which gives $\mu = 50\,265$ Hz. The eigenfrequency is $f_0 = 37.26$ MHz, as seen from Fig. 2 in the linear regime. The nonlinearity α is estimated from the shift[9]

$$\delta f(B) = f_{\max}(B) - f_0 = \frac{3\alpha[\Lambda_0(B)]^2}{32\pi^2 f_0}, \tag{5}$$

in frequency $f_{\max}$ at maximum amplitude in Fig. 2. In zero order the displacement of the beam is given by $\Lambda_0 = lI_0B/(4\pi f_0 \mu m_{\text{eff}})$. Relation (5) yields with $I_0 = 1.9 \times 10^{-5}$ A, a value of $\alpha = 9.1 \times 10^{28}\,(\text{ms})^{-2}$.

We first computed $x(t)$ by numerical integration of the Duffing equation with driving (2) and $F_1 = F_2 = lBI_0/m_{\text{eff}}$, $I_0 = 2.9 \times 10^{-5}$ A. We then calculated the power spectrum from the Fourier transform $\hat{x}(\omega)$ of $x(t)$ for large times (beyond the transient regime). For a direct comparison with the measured power P in Fig. 3, we employ $P \simeq RI_{\text{ap}}^2$. Here, R is the resistance of the electromechanical circuit and $I_{\text{ap}} = [4\pi f_0 \mu m_{\text{eff}}/(lB)]\hat{x}(\omega)$ the applied current, in close analogy to the zero-order relation between displacement Λ_0 and I_0.

The numerically obtained power spectra are displayed in Fig. 4. The positions of the measured satellite peaks, $f_i \pm n\Delta f$, *and* their amplitudes, are in good agreement with the numerical simulations for the entire parameter range shown. Even small modulations in the peak heights to the left of the two central peaks in Fig. 3(b) seem to be reproduced by the calculations in Fig. 4(b).

The numerical results in Fig. 4(a) show clearly the evolution of an increasing number of peaks with growing magnetic field, i.e., increasing driving amplitude. As in the experiment, the spectra exhibit an asymmetry in number and height of the satellite peaks which switches from lower to higher frequencies by increasing the magnetic field from 8 to 12 T. This behavior can be understood from Eq. (5) predicting a shift δf in resonance frequency with increasing magnetic field. This shift is reflected in the crossover in Figs. 3(a) and 4(a). For $B = 8$ T, the amplitudes of the satellite peaks are larger on the left than on the right side of the two central peaks. As the field is increased the frequency shift drives the right-hand-side satellites into resonance, increasing their heights.

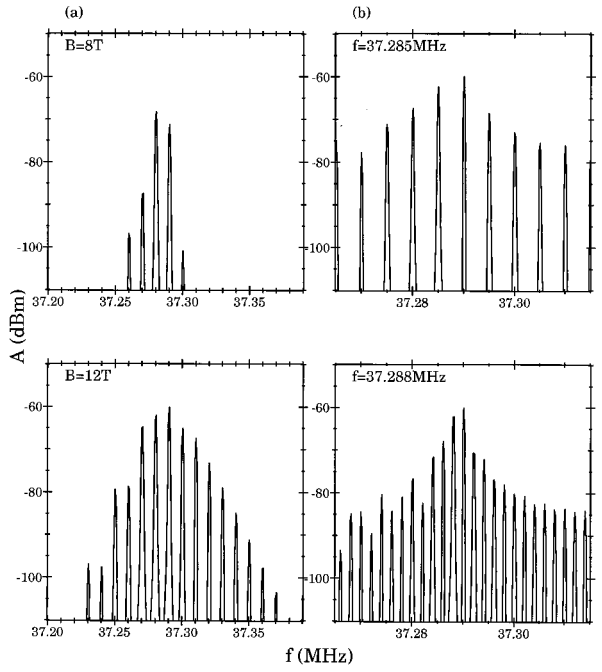

FIG. 4. Calculation of the power spectra from the numerical solution of Eqs. (1) and (2) for the same driving frequencies as used in Fig. 3. (a) Variation of magnetic field $B = 4$, 8, 9, 10, 11, and 12 T. (b) Variation of offset frequency at $B = 12$ T. Note that the two central peaks of Fig. 3 are not reproduced by the theory, since they stem from the reflected input signal.

In summary, we have shown how to employ the nonlinear response of a strongly driven nanomechanical resonator as a mechanical mixer in the radio-frequency regime. This opens up a wide range of applications, especially for signal processing. The experimental results are in very good agreement with numerical calculations based on a generalized Duffing equation, a prototype of a nonlinear oscillator.

The authors acknowledge financial support by the Deutsche Forschungsgemeinschaft (DFG).

[1] D. Rugar and P. Grütter, Phys. Rev. Lett. **67**, 699 (1991).
[2] D. S. Greywall, B. Yurke, P. A. Busch, A. N. Pargellis, and R. L. Willett, Phys. Rev. Lett. **72**, 2992 (1994).
[3] A. N. Cleland and M. L. Roukes, Appl. Phys. Lett. **69**, 2653 (1996).
[4] D. W. Carr and H. G. Craighead, J. Vac. Sci. Technol. B **15**, 2760 (1997); D. W. Carr, L. Sekaric, and H. G. Craighead, *ibid.* **16**, 3821 (1998).
[5] A. Erbe, R. H. Blick, A. Tilke, A. Kriele, and J. P. Kotthaus, Appl. Phys. Lett. **73**, 3751 (1998).
[6] L. Pescini, A. Tilke, R. H. Blick, H. Lorenz, J. P. Kotthaus, W. Eberhardt, and D. Kern, Nanotechnology **10**, 418 (1999).
[7] H. Krömmer, A. Erbe, A. Tilke, S. M. Manus, and R. H. Blick, Europhys. Lett. **50**, 101 (2000).
[8] U. Parlitz and W. Lauterborn, Phys. Lett. **107A**, 351 (1985).
[9] A. H. Nayfeh and D. T. Mook, *Nonlinear Oscillations* (Wiley-Interscience, New York, 1995).